

Hydrido-Ruthenium Cluster Complexes as Models for Reactive Surface Hydrogen Species of Ruthenium Nanoparticles. Solid-State ^2H NMR and Quantum Chemical Calculations

Torsten Gutmann,[†] Bernadeta Walaszek,[‡] Xu Yeping,[†] Maria Wächtler,[§] Iker del Rosal,^{||} Anna Grünberg,[†] Romuald Poteau,^{||} Rosa Axet,[⊥] Guy Lavigne,[⊥] Bruno Chaudret,[⊥] Hans-Heinrich Limbach,[#] and Gerd Buntkowsky^{*†}

Institut für Physikalische Chemie, Technische Universität Darmstadt, Petersenstrasse 20, D-64287 Darmstadt, Germany, Physikalisch-Technische Bundesanstalt, Abbestrasse 2-12, D-10587 Berlin, Germany, Institut für Physikalische Chemie, Friedrich-Schiller Universität Jena, Helmholtzweg 4, D-07743 Jena, Germany, Université de Toulouse, INSA, UPS, CNRS, LPCNO, 135 avenue de Rangueil, F-31077 Toulouse, France, Laboratoire de Chimie de Coordination du CNRS, 205, Route de Narbonne, 31077 Toulouse Cedex 04, France, and Institut für Physikalische und Theoretische Chemie, Freie Universität Berlin, Takustrasse 3, D-14195 Berlin, Germany

Received May 17, 2010; E-mail: gerd.buntkowsky@chemie.tu-darmstadt.de

Abstract: The ^2H quadrupolar interaction is a sensitive tool for the characterization of deuterium–metal binding states. In the present study, experimental solid-state ^2H MAS NMR techniques are used in the investigations of two ruthenium clusters, $\text{D}_4\text{Ru}_4(\text{CO})_{12}$ (**1**) and $\text{D}_2\text{Ru}_6(\text{CO})_{18}$ (**2**), which serve as model compounds for typical two-fold, three-fold, and octahedral coordination sites on metal surfaces. By line-shape analysis of the ^2H MAS NMR measurements of sample **1**, a quadrupolar coupling constant of 67 ± 1 kHz, an asymmetry parameter of 0.67 ± 0.1 , and an isotropic chemical shift of -17.4 ppm are obtained. In addition to the neutral complex, sample **2** includes two ionic clusters, identified as anionic $[\text{DRu}_6(\text{CO})_{18}]^-$ (**2⁻**) and cationic $[\text{D}_3\text{Ru}_6(\text{CO})_{18}]^+$ (**2⁺**). By virtue of the very weak quadrupolar interaction (<2 kHz) and the strong low-field shift ($+16.8$ ppm) of **2⁻**, it is shown that the deuteron is located in the symmetry center of the octahedron spanned by the six ruthenium atoms. For the cationic **2⁺**, the quadrupolar interaction is similar to that of the neutral **2**. Quantum chemical DFT calculations at different model structures for these ruthenium clusters were arranged in order to help in the interpretation of the experimental results. It is shown that the ^2H nuclear quadrupolar interaction is a sensitive tool for distinguishing the binding state of the deuterons to the transition metal. Combining the data from the polynuclear complexes with the data from mononuclear complexes, a molecular ruler for quadrupolar interactions is created. This ruler now permits the solid-state NMR spectroscopic characterization of deuterium adsorbed on the surfaces of catalytically active metal nanoparticles.

1. Introduction

The interaction of hydrogen with metal single-crystal surfaces has been extensively studied in surface science.¹ During the adsorption process, dihydrogen molecules are first physisorbed to the surfaces and in a second step chemisorbed. Generally, this process consists of a dissociation of the dihydrogen molecule. The atoms can then form bonds to one or more surface atoms and/or diffuse into the metal lattice, as illustrated schematically in Figure 1. In the case of Ru, it is now commonly

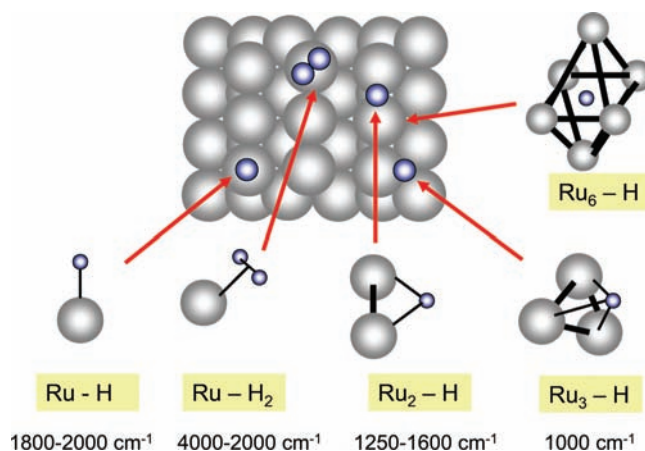


Figure 1. Hydrogen species on metal surfaces. The frequencies, in cm^{-1} , refer to hydrogenic vibrations. For further explanation see text.

[†] Technische Universität Darmstadt.

[‡] Physikalisch-Technische Bundesanstalt.

[§] Friedrich-Schiller Universität Jena.

^{||} Université de Toulouse.

[⊥] Laboratoire de Chimie de Coordination du CNRS.

[#] Freie Universität Berlin.

(1) Christmann, K. In *Hydrogen Transfer Reactions*; Hynes, J. T., Klinman, J., Limbach, H. H., Schowen, R. L., Eds.; Wiley-VCH: Weinheim, 1997.

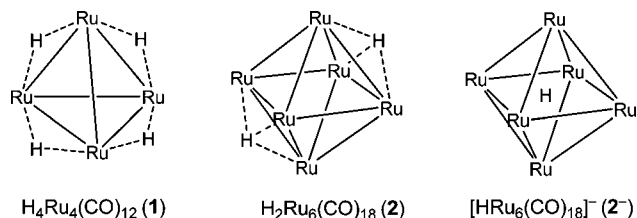


Figure 2. Molecular structure of model clusters 1, 2, and 2^- .

accepted that hydrogen atoms occupy three-fold coordinated face-centered cubic and hexagonal close-packed sites at all coverages.^{2–6} However, hydrogen atoms may also be located in two-fold sites, forming Ru_2H surface species, or “on top”, i.e. bound to a single metal atom.^{7,8} This assumption has recently been reinforced in the case of ruthenium nanoparticles by density functional theory (DFT)-based assignment of their solid-state ^2H MAS NMR spectra.⁹ In one case, i.e. palladium, evidence for nondissociated chemisorbed dihydrogen bound to a single metal atom has been observed.¹⁰

An important method to characterize the binding of hydrogen in surface sites has been vibrational spectroscopy, as the different surface sites exhibit different hydrogenic vibrational frequencies. Thus, for molecular H_2 bound to Pd, a vibrational frequency of 3700 cm^{-1} has been observed,¹⁰ whereas for tungsten dihydrogen complexes a value around 2700 cm^{-1} was found.¹¹ By contrast, the IR spectra of RuHL_n complexes as models for terminal hydrogens (“on top”) exhibit hydrogenic vibrations in the range of $1800\text{--}2000\text{ cm}^{-1}$. On the other hand, the corresponding vibrations for edge-bridging hydrogens, i.e. two-fold surface sites, should give rise to vibrational frequencies between 1250 and 1600 cm^{-1} ,^{12,13} as revealed by the model complex $\text{H}_4\text{Ru}_4(\text{CO})_{12}$ (1, Figure 2). Finally, the face-bridging hydrogens of $\text{H}_2\text{Ru}_6(\text{CO})_{18}$ (2, Figure 2), which represent models for three-fold surface sites, are characterized by red-shifted vibrational frequencies of about 1000 cm^{-1} .^{12,14}

In past years, metal nanoparticles have found widespread application as real catalysts in various heterogeneous and homogeneous reactions (see for example refs 15–17 and references therein). These particles typically consist of more or

less spherical metal particles containing several hundred atoms. They contain large organic surface ligands or are embedded in organic matrices. As compared to model metal surfaces, characterization of surface hydrogen species is difficult using conventional surface techniques including vibrational spectroscopy. However, recently, some of us have shown that interesting information about surface hydrogen on Ru nanoparticles can be obtained by variable-temperature solid-state ^2H NMR.^{18,19} Using this method, one can obtain deuteron quadrupolar coupling constants Q_{cc} and the asymmetry parameters η which provide information about electric field gradients (EFGs), which are also widely used for structural and dynamical studies.^{20–24} They are mainly determined by bond directions and charge distributions of electrons, which depend on the type of binding situation. The quadrupolar and chemical shift tensors can be interpreted by employing quantum chemical DFT calculations.^{21,25–33} In addition, anisotropic or isotropic motions can be detected which lead to a partial or full averaging of the quadrupole coupling tensor. Such an averaging was observed for deuterons on Ru nanoparticles at room temperature, whereas at low temperatures the intrinsic quadrupole coupling constants were obtained.³⁴ Using this method, also surface CD_3 groups on Ru nanoparticles created by reaction with ethene could be detected.¹⁹ Here solid-state ^2H NMR is clearly advantageous over solid-state ^1H NMR due to the presence of the organic linkers necessary to stabilize the nanoparticles, which cause very strong ^1H background signals.

During these studies the question came up whether the values of the deuteron quadrupole coupling tensors represent diagnostic tools for the characterization of the type of hydrogen surface species. In order to answer this question it is necessary to study a large range of different model systems. In previous studies we had performed variable-temperature solid-state ^2H NMR

- (2) Feulner, P.; Menzel, D. *Surf. Sci.* **1985**, *154*, 465.
 (3) Chou, M. Y.; Chelikowsky, J. R. *Phys. Rev. Lett.* **1987**, *59*, 1737.
 (4) Lindroos, M.; Pfnur, H.; Feulner, P.; Menzel, D. *Surf. Sci.* **1987**, *180*, 237.
 (5) Sokolowski, M.; Koch, T.; Pfnur, H. *Surf. Sci.* **1991**, *243*, 261.
 (6) Feibelman, P. J.; Houston, J. E.; Davis, H. L.; Oneill, D. G. *Surf. Sci.* **1994**, *302*, 81.
 (7) Lauth, G.; Schwarz, E.; Christmann, K. *J. Chem. Phys.* **1989**, *91*, 3729.
 (8) Doell, R.; Hammer, L.; Heinz, K.; Bedurftig, K.; Muschiol, U.; Christmann, K.; Seitsonen, A. P.; Bludau, H.; Over, H. *J. Chem. Phys.* **1998**, *108*, 8671.
 (9) Truffandier, L. A.; Del Rosal, I.; Chaudret, B.; Poteau, R.; Gerber, I. C. *Chemphyschem* **2009**, *10*, 2939.
 (10) Schmidt, P. K.; Christmann, K.; Kresse, G.; Hafner, J.; Lischka, M.; Gross, A. *Phys. Rev. Lett.* **2001**, *87*, 8709.
 (11) Kubas, G. J.; Ryan, R. R.; Swanson, B. I.; Vergamini, P. J.; Wasserman, H. J. *J. Am. Chem. Soc.* **1984**, *106*, 451.
 (12) Ishikawa, H.; Kondo, J. N.; Domen, K. *J. Phys. Chem.* **1999**, *B 103*, 3229.
 (13) Knox, S. A. R.; Koepke, J. W.; Andrews, M. A.; Kaesz, H. D. *J. Am. Chem. Soc.* **1975**, *97*, 3942.
 (14) Andrews, J. A.; Jayasooriya, U. A.; Oxtton, I. A.; Powell, D. B.; Sheppard, N.; Jackson, P. F.; Johnson, B. F. G.; Lewis, J. *Inorg. Chem.* **1980**, *19*, 3033.
 (15) Reetz, M. T.; Westermann, E. *Angew. Chem., Int. Ed.* **2000**, *39*, 165.
 (16) Roucoux, A.; Schulz, J.; Patin, H. *Chem. Rev.* **2002**, *102*, 3757.
 (17) Roucoux, A.; Philippot, K. In *Handbook of Homogenous Hydrogenations*; de Vries, G., Ed.; Wiley-VCH: Weinheim, 2007, p 217.

- (18) Pery, T.; Pelzer, K.; Buntkowsky, G.; Philippot, K.; Limbach, H. H.; Chaudret, B. *ChemPhysChem.* **2005**, *6*, 605.
 (19) Garcia-Anton, J.; Axet, M. R.; Jansat, S.; Philippot, K.; Chaudret, B.; Pery, T.; Buntkowsky, G.; Limbach, H. H. *Angew. Chem., Int. Ed.* **2008**, *47*, 2074.
 (20) del Rosal, I.; Gutmann, T.; Maron, L.; Jolibois, F.; Chaudret, B.; Walaszek, B.; Limbach, H. H.; Poteau, R.; Buntkowsky, G. *Phys. Chem. Chem. Phys.* **2009**, *11*, 5657.
 (21) Mirzaei, M.; Hadipour, N. L. *Chem. Phys. Lett.* **2007**, *438*, 304.
 (22) Mirzaei, M.; Hadipour, N. L. *J. Comput. Chem.* **2008**, *29*, 832.
 (23) Walaszek, B.; Adamczyk, A.; Pery, T.; Yeping, X.; Gutmann, T.; Amadeu de Sousa, N.; Ulrich, S.; Breitzke, H.; Vieth, H. M.; Sabo-Etienne, S.; Chaudret, B.; Limbach, H.-H.; Buntkowsky, G. *J. Am. Chem. Soc.* **2008**, *130*, 17502.
 (24) Wong, A.; Ida, R.; Mo, X.; Gan, Z. H.; Poh, J.; Wu, G. *J. Phys. Chem. A* **2006**, *110*, 10084.
 (25) Autschbach, J. In *Density functional theory in inorganic chemistry*; Kaltsoyannis, N.; McGrady, J. E., Eds.; Springer Verlag: Berlin/Heidelberg, 2004; Vol. 112, p 1.
 (26) Behzadi, H.; Hadipour, N. L.; Mirzaei, M. *Biophys. Chem.* **2007**, *125*, 179.
 (27) del Rosal, I.; Maron, L.; Poteau, R.; Jolibois, F. *Dalton Trans.* **2008**, 3959.
 (28) Gutmann, T.; Schweitzer, A.; Waechter, M.; Breitzke, H.; Buchholz, A.; Plass, W.; Buntkowsky, G. *Z. Phys. Chem.* **2008**, *222*, 1389.
 (29) Pavanello, M.; Mennucci, B.; Tomasi, J. *Theor. Chem. Acc.* **2006**, *116*, 711.
 (30) Schweitzer, A.; Gutmann, T.; Waechter, M.; Breitzke, H.; Buchholz, A.; Plass, W.; Buntkowsky, G. *Solid State Nucl. Magn.* **2008**, *34*, 52.
 (31) Jolibois, F.; Soubias, O.; Reat, V.; Milon, A. *Chemistry* **2004**, *10*, 5996.
 (32) Macholl, S.; Boerner, F.; Buntkowsky, G. *Z. Phys. Chem.* **2003**, *217*, 1473.
 (33) Truffandier, L.; Paris, M.; Payen, C.; Boucher, F. *J. Phys. Chem. B* **2006**, *110*, 21403.
 (34) Wehrmann, F.; Fong, T.; Morris, R. H.; Limbach, H.-H.; Buntkowsky, G. *Phys. Chem. Chem. Phys.* **1999**, *1*, 4033.

experiments on mononuclear transition metal complexes in which one D_2 is bound to W^{35} or to Ru^{34} or several dihydrogen molecules are bound to Ru .²³ However, model studies of the other surface species depicted in Figure 1 were still lacking. In this study, we have tried to fill this gap by a solid-state 2H NMR study of the two model complexes **1** and **2** depicted in Figure 2. For the latter compound, the deprotonated anion 2^- has been observed in solution.³⁶ Our main interest was the experimental determination of the quadrupolar coupling constants Q_{cc} and the asymmetry parameter η for the fully deuterated complexes $D_4Ru_4(CO)_{12}$ (**1**) and $D_2Ru_6(CO)_{18}$ (**2**), as well as the exploration of solid-state properties of 2^- . In the first step, these compounds were studied by a combination of solid-state 2H magic-angle spinning (MAS) at ambient temperatures and 2H line shape analysis at low temperatures. These measurements revealed the experimental quadrupolar and chemical shift parameters and also the presence of molecular motions. In the second step, these parameters were compared to the calculated solid-state NMR parameters. Our DFT calculations, which are mainly intended to interpret the experimental data, were performed at the B3LYP/6-31++G(d,p) level of theory. A deeper theoretical analysis will be given in a subsequent paper.

The rest of the paper is organized as follows: after the present Introduction, the theory of 2H solid-state NMR is shortly summarized, and then the sample preparation and a short overview of the characterization are given. The solid-state 2H NMR spectra and their simulations are discussed, followed by the results of quantum chemical DFT calculations of the two ruthenium clusters, which are interpreted in terms of the experimental data.

2. Materials and Methods

2.1. Solid-State 2H NMR. The basic theory of solid-state 2H NMR is well-documented³⁷ and only shortly summarized here.

In solid-state 2H NMR, the leading interaction is the quadrupolar interaction, which is described in high-field approximation by the quadrupolar Hamiltonian for spin $I = 1$,

$$\hat{H}_Q = 2\pi\nu_Q(\vartheta, \varphi)\left(\hat{I}_z^2 - \frac{2}{3}\right) \quad (1)$$

where \hat{I}_z is the angular momentum operator in the z -direction. The orientation-dependent resonance frequencies ν_Q are given by

$$\nu_Q(\vartheta, \varphi) = \pm \frac{3}{4}Q_{cc}\frac{1}{2}(3\cos^2\vartheta - 1 - \eta\sin^2\cos 2\varphi) \quad (2)$$

The quadrupolar coupling constant Q_{cc} , respectively the quadrupolar splitting Q_{zz} as a measure for the strength of the quadrupolar interaction, is obtained from the experiment as

$$Q_{cc} = \frac{4}{3}Q_{zz} = \frac{eQV_{zz}}{h} \quad (3)$$

where Q is the quadrupolar moment ($Q = 0.00286$ barns for deuterons), V_{zz} represents the largest principal component of the EFG tensor, η is the asymmetry parameter, which gives information about the symmetry of the EFG, and ϑ and φ are the azimuthal and polar angles of the quadrupolar principal axis system (PAS)

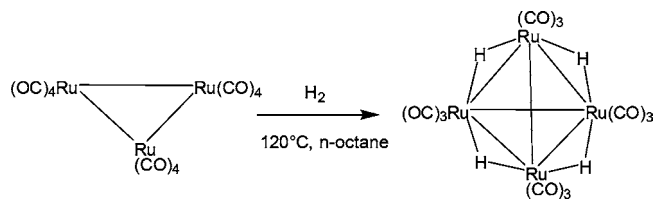


Figure 3. Synthesis of $H_4Ru_4(CO)_{12}$.

with respect to the external magnetic field B_0 . Under MAS conditions, the anisotropy of the quadrupolar interaction gives rise to a typical spinning sideband pattern centered around the line at the value of the isotropic chemical shift.

2.2. Experimental Details. All static experiments were performed at a field of 7.03 T, corresponding to a 2H resonance frequency of 46.03 MHz. An Oxford wide-bore magnet (89 mm) equipped with a room-temperature shim unit was used. The home-built three-channel spectrometer was described previously by some of us.^{34,38} For the experiments, a home-built 5 mm 2H NMR probe was used. Low-temperature measurements were performed in a dynamic Oxford CF1200 helium flow cryostat. An Oxford ITC 503 temperature controller was used to control the temperature. The typical 90° pulse width was 4.5 μs . Solid echo technique with an echo spacing of 30 μs was utilized. The repetition time of the experiments was chosen between 1 and 10 s, depending on the T_1 relaxation time of the samples. To acquire the deuterium powder patterns in these samples with reasonable signal-to-noise ratio, nearly 2000 scans per spectrum were accumulated.

2H MAS NMR spectra were recorded on a Varian InfinityPlus (14 T, 2H : 92.1 MHz) with a Chemagnetics HX 4 mm probe. A pulse sequence with the 90° pulse of 2.1 μs and 4 s of delay time was used. The measurements on the 600 MHz spectrometer employed the external chemical shift of standard deuterated water (set to +4.7 ppm) as chemical shift reference. The simulations were done using a laboratory-written program based on genetic algorithms (GA) described elsewhere.³⁹

2.3. Sample Preparation. 2.3.1. $H_4Ru_4(CO)_{12}$ (1**).** The $H_4Ru_4(CO)_{12}$ and $D_4Ru_4(CO)_{12}$ clusters⁴⁰ were prepared by a modification of the original published procedure, which involves direct bubbling of hydrogen in a solution of $Ru_3(CO)_{12}$ in n -octane under reflux (see Figure 3).¹³ In order to avoid losses that would result from bubbling the expensive D_2 gas in an open system, both the hydrogenation and the deuteration of $Ru_3(CO)_{12}$ were performed in Fischer & Porter glassware reactors. Samples of $Ru_3(CO)_{12}$ (175 mg), prepared by a published procedure,⁴¹ were introduced in a 50 mL Fischer & Porter tube equipped with a magnetic stirrer. n -Octane (8 mL) was added, and the solution was degassed under reduced pressure. The tube was then placed under 5 atm of H_2 (or D_2) and immersed into an oil bath heated at 120 $^\circ C$ for 3 h. At that stage, a characteristic violet color was detected, indicative of the formation of the intermediate complex $H_2Ru_4(CO)_{13}$ as a contaminant of the final product $H_4Ru_4(CO)_{12}$. The solution was thus allowed to cool to room temperature, the tube was opened, and a nitrogen gas inlet was introduced. Nitrogen was bubbled through the solution for 10 min to evacuate the released CO. The tube was then loaded again with 5 atm of H_2 (or D_2) and heated at 120 $^\circ C$ for 3 h more. The same operation was repeated one more time, which resulted in complete conversion of the intermediate complex into the final product $H_4Ru_4(CO)_{12}$ after a total reaction time of 9 h. It is noteworthy that such a stepwise procedure was not required

(35) Wehrmann, F.; Albrecht, J.; Gedat, E.; Kubas, G. J.; Limbach, H. H.; Buntkowsky, G. *J. Phys. Chem. A* **2002**, *106*, 2855.

(36) Eady, C. R.; Johnson, B. F. G.; Lewis, J.; Malatesta, M. C.; Machin, P.; Mcpartlin, M. *J. Chem. Soc., Chem. Commun.* **1976**, 945.

(37) Schmidt-Rohr, K.; Spiess, H. W. *Multidimensional Solid State NMR and Polymers*; Academic Press: London, 1994.

(38) Gedat, E.; Schreiber, A.; Albrecht, J.; Shenderovich, I.; Findenegg, G.; Limbach, H.-H.; Buntkowsky, G. *J. Phys. Chem. B* **2002**, *106*, 1977.

(39) Waechter, M.; Schweitzer, A.; Gutmann, T.; Breitzke, H.; Buntkowsky, G. *Solid State Nucl. Magn.* **2009**, *35*, 37.

(40) Wilson, R. D.; Wu, S. M.; Love, R. A.; Bau, R. *Inorg. Chem.* **1978**, *17*, 1271.

(41) Fauré, M.; Saccavini, C.; Lavigne, G. *Chem. Commun.* **2003**, 1578.

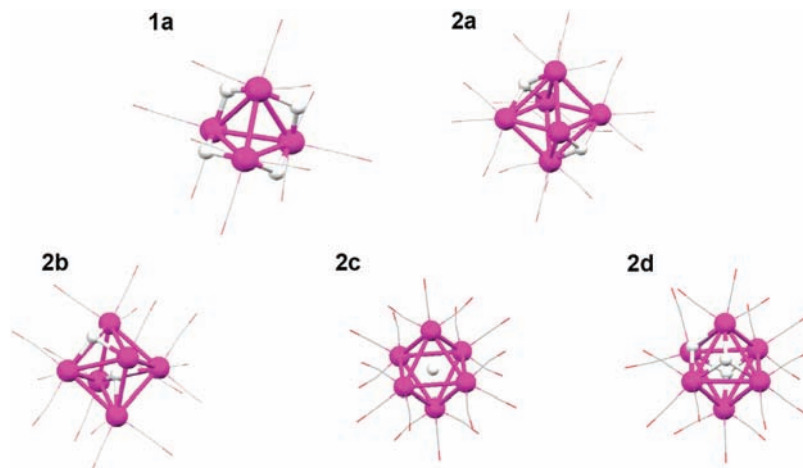


Figure 4. Molecular structures resulting from the DFT calculations of the clusters $\text{H}_4\text{Ru}_4(\text{CO})_{12}$ (**1**), $\text{H}_2\text{Ru}_6(\text{CO})_{18}$ (**2**), $[\text{H}_3\text{Ru}_6(\text{CO})_{18}]^+$ (2^+), and $[\text{HRu}_6(\text{CO})_{18}]^-$ (2^-). The latter contains a deuteron inside the Ru_6 octahedron (see section 2.5 for details).

in the initial published procedure carried out in an open system, since CO was then released along with the continuous H_2 stream bubbled into the flask. A considerable advantage of using a Fischer & Porter tube is indeed to minimize the amount of expensive D_2 . The solution was then allowed to cool to room temperature overnight. This allowed quantitative precipitation of characteristic yellow crystals of the cluster $\text{H}_4\text{Ru}_4(\text{CO})_{12}$ (or $\text{D}_4\text{Ru}_4(\text{CO})_{12}$) which were subsequently filtered and dried under vacuum. To protect the clusters from oxygen, the samples were placed in 5 mm NMR glass tubes under an argon atmosphere.

2.3.2. $\text{H}_2\text{Ru}_6(\text{CO})_{18}$ (2**).** Several methods have been described in the literature for the preparation of $\text{H}_2\text{Ru}_6(\text{CO})_{18}$, all involving a reduction of $\text{Ru}_3(\text{CO})_{12}$. In the first one, the reduction was achieved with the mononuclear carbonyl anions $[\text{Mn}(\text{CO})_5]^-$. After acidification, extraction of the reaction mixture with dichloromethane allowed the formation of the complex, albeit in a very low yield.⁴¹ The second published procedure employed the reaction of $\text{Ru}_3(\text{CO})_{12}$ with a base (KOH/MeOH), leading to either $[\text{HRu}_3(\text{CO})_{11}]^-$ or $[\text{Ru}_6(\text{CO})_{18}]^{2-}$, depending upon reaction conditions. Acidification of both products was then found to give $[\text{HRu}_6(\text{CO})_{18}]^-$, whereas further acidification in basic solvents such as THF gave $\text{H}_2\text{Ru}_6(\text{CO})_{18}$ in quantitative yields.⁴² However, the most convenient method, which was used in the present case, is the one described by Shore, using alkali metal–benzophenone as reducing agent.⁴³ The advantage is that it produces selectively the dianion $[\text{Ru}_6(\text{CO})_{18}]^{2-}$. The latter is then protonated with an ether solution of either HCl or DCl, producing $\text{H}_2\text{Ru}_6(\text{CO})_{18}$ or $\text{D}_2\text{Ru}_6(\text{CO})_{18}$, respectively. Further treatment of these clusters with 1 equiv of a titrated methanolic solution of NET_4OH gives the monoanionic species $[\text{HRu}_6(\text{CO})_{18}]^-$ or $[\text{DRu}_6(\text{CO})_{18}]^-$, respectively.

2.4. Sample Characterization. 2.4.1. $\text{H}_4\text{Ru}_4(\text{CO})_{12}$ (1**).** The structure of $\text{H}_4\text{Ru}_4(\text{CO})_{12}$ is shown Figure 2. In the literature,⁴⁰ this cluster is presented with D_{2d} symmetry containing two kinds of metal–carbon bonds. The longer metal–carbon bonds are in positions opposite the unbridged Ru–Ru bond ($\text{Ru–C} = 1.938 \text{ \AA}$ average), and the shorter ones are opposite the bridged Ru–H–Ru bond ($\text{Ru–C} = 1.902 \text{ \AA}$ average). All carbonyl groups are coordinated essentially linearly. The assumptions that the four long Ru–Ru distances correspond to Ru–H–Ru bonds, and the two short Ru–Ru distances correspond to unbridged Ru–Ru bonds, are reasonable. Thus, we performed quantum chemical calculations with the hydrogens positioned between Ru(1)–Ru(3), Ru(2)–Ru(3), Ru(1)–Ru(4), and Ru(2)–Ru(4).⁴⁰

Solid-state ^1H and ^{13}C NMR studies of **1** published in 1994 by Aime et al.⁴⁴ pointed out that the hydrides are involved in a dynamic process. However, the motion of the hydrides does not involve the motion of CO ligands. Consequently, they proposed two possible processes, namely (i) a rotation of the whole Ru_4 core around the C_2 axis passing through the midpoints of the Ru(1)–Ru(2) and Ru(3)–Ru(4) bonds and (ii) jumps of the hydride ligands between the four equivalent positions. Later, an alternative motional model for hydrides in this cluster was proposed by Harding et al.⁴⁵ A detailed analysis of the motional properties of the hydride ligands is currently in progress in our laboratory.

2.4.2. $\text{H}_2\text{Ru}_6(\text{CO})_{18}$ (2**).** The 86-electron cluster $\text{H}_2\text{Ru}_6(\text{CO})_{18}$ (**2**) displays a distorted octahedral metal geometry. Each ruthenium atom is coordinated by three terminal carbonyl ligands.^{42,46}

Due to the fact that the hydride ligands are invisible in the X-ray structure, their position was estimated by DFT calculations. Churchill et al.⁴⁶ have proposed a structure where each hydride ligand is directly coordinated in the center of a facet of the octahedron formed by three ruthenium atoms (Figure 4, **2a**). In our calculations we found an alternative possible structure (**2b**), where only one hydrogen is located in the center of a facet, and the second is centered inside the Ru_6 octahedron.

2.5. Computational Details. The quantum chemical calculations were done with Gaussian03 under the Linux environment using DFT. All calculations of chemical shift and EFG tensors were performed using Becke's three-parameter hybrid functional^{47,48} along with the Lee–Yang–Parr correlation functional⁴⁹ (B3LYP). For pre-optimizing the structures, Dunning's double- ζ basis set SDD⁵⁰ was used for all atoms except Ru, for which a Gaussian basis set was utilized, generated from an averaged relativistic effective potential (AREP).⁵¹ In the final calculations, Pople's double- ζ basis set,^{52,53} combining d- and p-polarization functions and diffuse

(42) Jackson, P. F.; Johnson, B. F. G.; Lewis, J.; Mcpartlin, M.; Nelson, W. J. *J. Chem. Soc., Chem. Commun.* **1979**, 735.

(43) Bhattacharyya, A. A.; Nagel, C. C.; Schore, S. G. *Organometallics* **1983**, *2*, 1187.

(44) Aime, S.; Gobetto, R.; Orlandi, A.; Groombridge, C. J.; Hawkes, G. E.; Mantle, M. D.; Sales, K. D. *Organometallics* **1994**, *13*, 2375.

(45) Harding, R. A.; Nakayama, H.; Eguchi, T.; Nakamura, N.; Heaton, B. T.; Smith, A. K. *Polyhedron* **1998**, *17*, 2857.

(46) Churchill, M. R.; Wormald, J.; Knight, J.; Mays, M. J. *J. Chem. Soc., Chem. Commun.* **1970**, 458.

(47) Becke, A. D. *J. Chem. Phys.* **1993**, *98*, 1372.

(48) Becke, A. D. *J. Chem. Phys.* **1993**, *98*, 5648.

(49) Lee, C. T.; Yang, W. T.; Parr, R. G. *Phys. Rev. B* **1988**, *37*, 785.

(50) Dunning, T. H.; Hay, P. J. *Modern Theoretical Chemistry*; Plenum: New York, 1976.

(51) Lajohn, L. A.; Christiansen, P. A.; Ross, R. B.; Atashroo, T.; Ermler, W. C. *J. Chem. Phys.* **1987**, *87*, 2812.

(52) Harihara, C.; Pople, J. A. *Theor. Chim. Acta* **1973**, *28*, 213.

(53) Hehre, W. J.; Ditchfield, R.; Pople, J. A. *J. Chem. Phys.* **1972**, *56*, 2257.

functions,⁵⁴ e.g. 6-31++G(d,p), as well as Ahlrich's triple- ζ basis sets TZV and TZVP^{55,56} were used for all atoms except Ru, for which AREP was applied. With these optimized structures the NMR calculations were done at the same level of theory using the GIAO^{57,58} method. Additional frequency analyses at the optimized structure were carried out to characterize the nature of stationary points.

Note that these basis sets and associated pseudopotentials differ from those reported in our previous work.²⁰ We have carefully checked for several mononuclear Ru complexes that Q_{cc} values do not differ much between the two levels of calculations, but they are systematically higher at the present level. The reverse situation is observed for chemical shifts which are slightly closer to experiments at the present level than in our previous work.⁵⁹

2.5.1. $D_4Ru_4(CO)_{12}$ (1). As starting structure for the pre-optimizations of $D_4Ru_4(CO)_{12}$, the X-ray structure measured by Wilson et al.⁴⁰ was used. Since the X-ray structure does not reveal the hydrogen positions, the missing deuterium atoms were added to the four edges of the distorted Ru_4 tetrahedron with the larger bond distances. The resulting structure (see Figure 4, structure **1a**) has nearly D_{2d} symmetry. It is almost degenerate ($\Delta E < 0.1$ kcal mol⁻¹) with the perfectly symmetric D_{2d} structure (**1b**) previously considered in ref 59. After pre-optimization of these starting structures, the $D_4Ru_4(CO)_{12}$ isomers were optimized with a larger basis set (6-31++G(d,p), TZV, and TZVP) to create the structures for the single-point NMR calculations.

2.5.2. $D_2Ru_6(CO)_{18}$ (2), $[D_3Ru_6(CO)_{18}]^+$ (2⁺**), and $[DRu_6(CO)_{18}]^-$ (**2⁻**).** To corroborate the interpretation of the MAS spectra, DFT calculations of the EFG and the CSA tensors at the ruthenium clusters $D_2Ru_6(CO)_{18}$ (**2**), $[D_3Ru_6(CO)_{18}]^+$ (**2⁺**), and $[DRu_6(CO)_{18}]^-$ (**2⁻**) were performed in the same way as the calculations of **1a**, employing the 6-31++G(d,p) basis set. Based on the X-ray structure of $D_2Ru_6(CO)_{18}$,⁴⁶ the two different starting structures **2a** and **2b** (Figure 4) were used for the optimization of the $D_2Ru_6(CO)_{18}$ cluster. For the $[DRu_6(CO)_{18}]^-$ cluster, the starting structure **2c** was assumed, where the deuterium is placed in the center of the Ru_6 octahedron. For the $[D_3Ru_6(CO)_{18}]^+$ cluster, the starting structure **2d** was chosen as starting structure, where each of the three deuterons is directly coordinated in the center of a facet of the octahedron formed by three rutheniums. Note that there exist also additional structures of this complex, two with the same binding situation as in **2d** and a third one that exhibits two face-capping deuterons and one interstitial deuterium, which will be described in detail in a subsequent paper.

3. Results and Discussion

3.1. $D_4Ru_4(CO)_{12}$ Cluster. 3.1.1. Solid-State 2H NMR Spectra. The small amounts of available sample together with the relatively long T_1 relaxation time render the samples relatively insensitive. Therefore, only MAS spectra and no static spectra were measured. The quadrupolar interaction parameters found by the line-shape analysis of these 2H MAS NMR spectra are collected in Table 3 (below).

To exclude the motional processes discussed above, the 2H MAS NMR spectra of **1** were measured at -100 °C. Figure 5 displays the 2H MAS NMR spectrum of **1** measured at a spinning rate of 4 kHz. The appearance of a single sideband pattern centered at an isotropic chemical shift value of -17.4

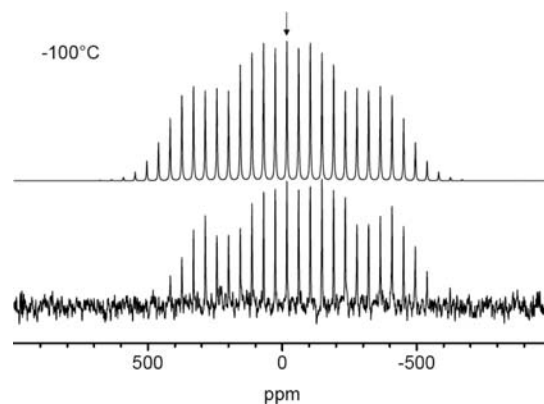


Figure 5. Solid-state 2H MAS NMR spectrum of the $D_4Ru_4(CO)_{12}$ (**1**) complex measured at 92.1 MHz and 4 kHz of spinning. Lower panel, experiment; upper panel, simulation with $Q_{cc} = 67 \pm 1$ kHz, $\eta = 0.67 \pm 0.1$.

ppm clearly shows that the sample includes only a single type of deuterons and thus is chemically clean. The large number of spinning sidebands permits a reliable determination of the spectral parameters. The analysis of the sideband pattern yields a quadrupolar coupling constant of $Q_{cc} = 67 \pm 1$ kHz and an asymmetry parameter of $\eta = 0.67 \pm 0.1$.

It is interesting to compare the values of the quadrupolar parameters of deuterium in the tetranuclear complex $D_4Ru_4(CO)_{12}$ to those of the mononuclear Ru–D type complexes studied in our previous publication.²³ In the case of the on-top Ru–D complexes, the quadrupolar coupling constant was approximately 90 kHz and the asymmetry parameter was < 0.1 . Compared to these values there are pronounced differences in the case of the tetranuclear $D_4Ru_4(CO)_{12}$ complex.

While the deuterium in $D_4Ru_4(CO)_{12}$ exhibits a strong asymmetry ($\eta = 0.7$), the asymmetry parameters of deuterium arranged on the top of the ruthenium atoms in the mononuclear complexes are very small ($\eta < 0.1$). This result can be understood by taking the local geometry in the vicinity of the deuterium into account. In the case of the mononuclear complexes, there is an approximately cylindrical symmetry around the Ru–D bond,^{20,23} which results in the axial symmetry of the tensor. In the case of the $D_4Ru_4(CO)_{12}$, however, there is a local planar geometry of the Ru–D–Ru edge, which breaks the axial symmetry and causes the large asymmetry of $\eta = 0.7$. Moreover, the binding to two metal centers reduces the size of the electric field gradient at the position of the deuterium, which is reflected in the smaller value of Q_{cc} . Thus, the investigations of the $D_4Ru_4(CO)_{12}$ cluster reveal that solid-state 2H MAS NMR clearly allows to distinguish between terminal and bridged bound surface species on the metal surface.

3.1.2. DFT Calculations. A first result which can be obtained from the optimization of **1a** is the most probable position of the deuterons in the $D_4Ru_4(CO)_{12}$ model complex (Figure 6a). The energy minimum of this complex is found for a structure with a distorted D_{2d} symmetry (Figure 6b), where the bridging deuterons, which are bound to two ruthenium atoms of the Ru_4 tetrahedron, are outside the planes of the Ru_3 facets. The calculations with the 6-31++G(d,p) basis set reveal angles of $17^\circ \pm 1^\circ$ between the Ru_3 and the Ru–D–Ru planes.

The results of the DFT calculations (Table 1) confirm the experimental values for the quadrupolar interaction parameters Q_{cc} and η of the deuterons. A relatively strong asymmetry in the range of 0.60–0.90 and a quadrupolar coupling constant in

(54) Clark, T.; Chandrasekhar, J.; Spitznagel, G. W.; Schleyer, P. V. *J. Comput. Chem.* **1983**, *4*, 294.

(55) Schäfer, A.; Horn, H.; Ahlrichs, R. *J. Chem. Phys.* **1992**, *97*, 2571.

(56) Schäfer, A.; Huber, C.; Ahlrichs, R. *J. Chem. Phys.* **1994**, *100*, 5829.

(57) Ditchfield, R. *Mol. Phys.* **1974**, *27*, 789.

(58) Wolinski, K.; Hinton, J. F.; Pulay, P. *J. Am. Chem. Soc.* **1990**, *112*, 8251.

(59) del Rosal, I.; Jolibois, F.; Maron, L.; Philippot, K.; Chaudret, B.; Poteau, R. *Dalton Trans.* **2009**, 2142.

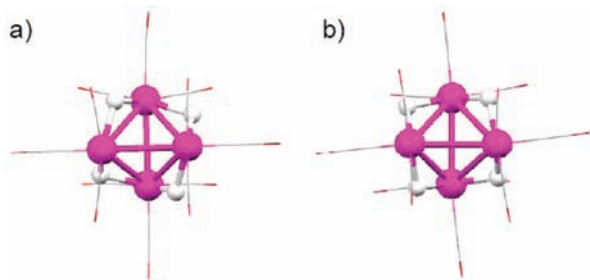


Figure 6. Structure of the Ru_4 tetrahedron cut from the $\text{D}_4\text{Ru}_4(\text{CO})_{12}$ (**1a**) complex with the four deuterons (a) forming a plane in each case with one of the Ru_3 faces and (b) out of the Ru_3 faces (optimized structure with the 6-31++G(d,p) basis set).

Table 1. Quadrupolar Coupling Constants Q_{cc} , Quadrupolar Splitting Q_{zz} , and Asymmetry Parameter η Averaged for the Four Deuteriums in the $\text{D}_4\text{Ru}_4(\text{CO})_{12}$ (**1a**) Complex, Calculated with Different Basis Sets at the B3LYP Level of Theory^a

basis set	structure 1a			optimized structure 1a		
	Q_{cc} (kHz)	Q_{zz} (kHz)	η	Q_{cc} (kHz)	Q_{zz} (kHz)	η
SDD	83.5	62.6	0.86	80.8	60.6	0.68
6-31++G(d,p)	81.4	61.1	0.83	79.3	59.5	0.65
TZV	81.4	61.1	0.88	78.4	58.8	0.70
TZVP	82.3	61.7	0.85	80.7	60.5	0.67
expt (−100 °C)				67		0.67

^a The two structures refer to those depicted in Figure 6.

the range of 78–84 kHz are calculated for **1a** and the optimized structure of **1a**. It is shown that the resulting Q_{cc} values are nearly independent of the employed basis set and the used structure. The latter is an indication that the structure of the heavy atoms is only slightly changed during the optimization. The theoretical quadrupolar parameters can be considered to be in good agreement with experiments, with an almost identical asymmetry parameter and a slightly overestimated Q_{cc} value. Quadrupolar parameters for **1b** ($Q_{cc} = 83$ kHz and $\eta = 0.6$ calculated at the B3LYP/6-31++G(d,p) level of theory) do not differ significantly from those calculated for **1a**, in agreement with the high structural similarity between these two isomers.

3.2. $\text{D}_2\text{Ru}_6(\text{CO})_{18}$ Cluster. 3.2.1. Solid-State MAS NMR Spectra. As a starting point for the study of the $\text{D}_2\text{Ru}_6(\text{CO})_{18}$ cluster, we also measured static solid-state ^2H NMR spectra. These spectra (not shown) revealed a very complicated line shape, which indicated the presence of several chemically inequivalent deuterons with different chemical shifts and quadrupolar couplings. For this reason we did not analyze these spectra further but employed solid-state ^2H MAS NMR instead, which permits to resolve the chemical shifts.

Figure 7a presents the experimental spectrum of $\text{D}_2\text{Ru}_6(\text{CO})_{18}$ measured at room temperature with a spinning speed of 4 kHz. It is evident that there are three strong components in the spectrum. Two different spinning speeds were used to identify the central signals. Due to the low number of spinning sidebands in the spectrum measured with a MAS speed of 6 kHz, only the spectrum at 4 kHz was employed for the analysis of the quadrupolar tensor.

In the 4 and 6 kHz MAS spectra, three different signal groups (Figure 7a,b) are found, with isotropic chemical shift values of −15.86, −20.9, and 16.8 ppm. For the assignment of these three signal groups the liquid-state NMR spectra (CD_2Cl_2) of the $\text{H}_2\text{Ru}_6(\text{CO})_{18}$ complex were employed.⁶⁰ The ^1H NMR spectrum of a dissolved $\text{H}_2\text{Ru}_6(\text{CO})_{18}$ single crystal exhibited only one sharp singlet at −15.6 ppm. On the basis of this result, we attribute the signal with the chemical shift of −15.86 ppm to deuterons from the $\text{D}_2\text{Ru}_6(\text{CO})_{18}$ cluster. The quadrupolar coupling constant and the asymmetry parameter were estimated by the line-shape analysis of the MAS sideband spectrum. The fitting revealed values of $Q_{cc} = 24.63$ kHz and $\eta = 0.2$, which are assigned to deuterium bonded to three ruthenium atoms.

The weaker signal group with an isotropic chemical shift of −20.9 ppm, which is also in the hydride region, is attributed to be a decomposition product which could refer to the protonated species $[\text{D}_3\text{Ru}_6(\text{CO})_{18}]^+$. Owing to the low concentration of this compound, we did not perform a full fit of the sideband spectrum. However, by comparison to the spectrum of $\text{D}_2\text{Ru}_6(\text{CO})_{18}$, it is evident that their quadrupolar interactions are similar to an estimated value of $Q_{cc} = 25 \pm 4$ kHz.

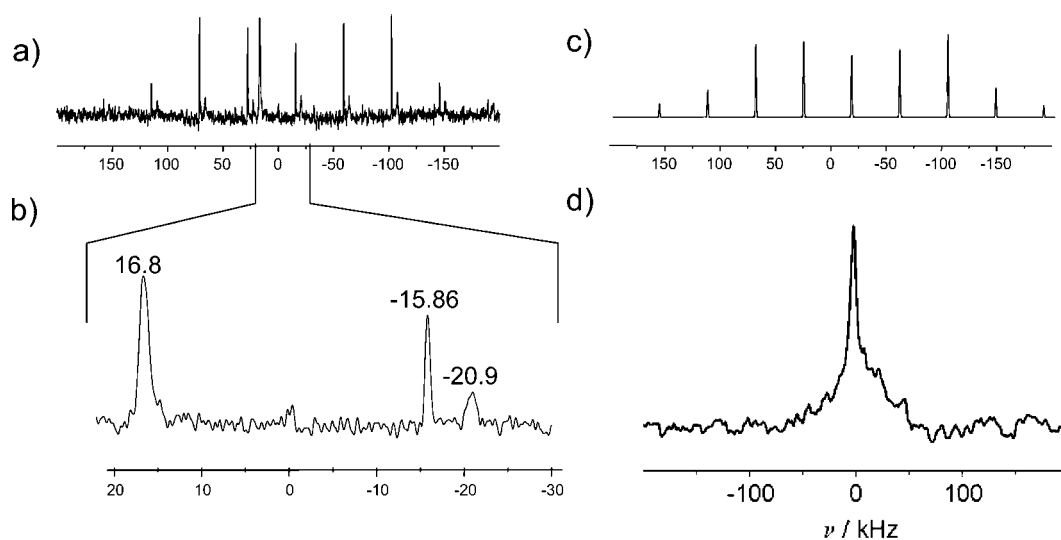


Figure 7. Solid-state ^2H NMR spectra of **2**: (a) Experimental MAS NMR spectrum measured at a spinning speed of 4 kHz and (b) center region of the experimental MAS spectra, where three different signals can be seen with chemical shift values of −15.86, −20.9, and 16.8 ppm. (c) Simulation of the main component at −15.86 ppm at 4 kHz. (d) Non-spinning 46.03 MHz ^2H NMR spectra of $\text{D}_2\text{Ru}_6(\text{CO})_{18}$ measured at 22 K. Note the presence of the narrow off-resonant line in the spectrum, indicating the presence of deuterons without quadrupolar interaction. Due to the low signal-to-noise ratio, caused by the low absolute amount of deuterium in the sample, no line shape analysis was performed.

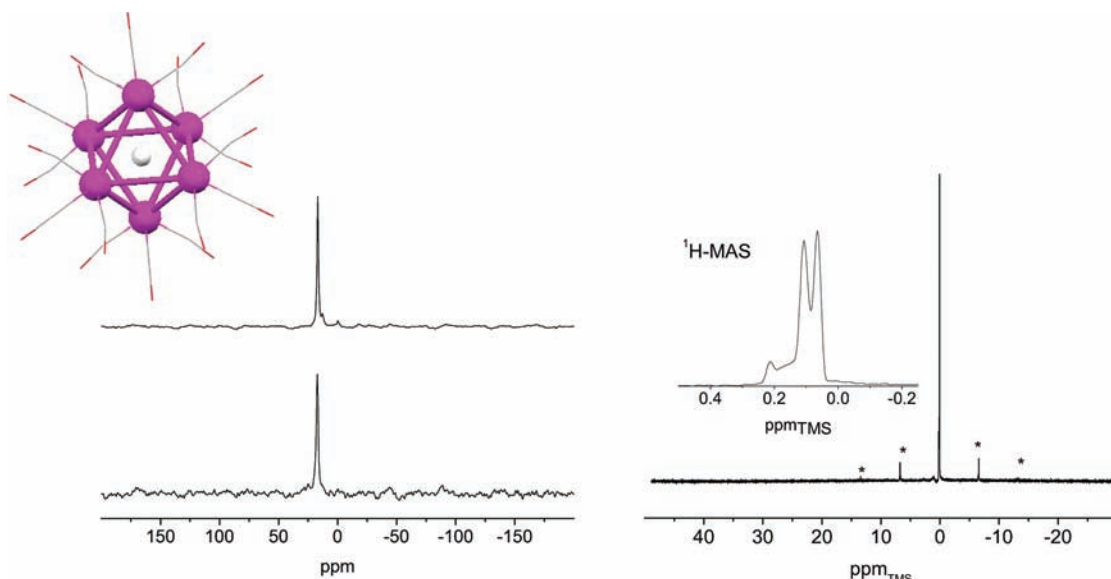


Figure 8. Left: ^2H MAS NMR (4 kHz spinning speed) spectra of solid $[\text{DRu}_6(\text{CO})_{18}]^-$. Note the absence of spinning side bands. Right: Room-temperature ^1H MAS NMR of solid $[\text{DRu}_6(\text{CO})_{18}]^-$. Note the absence of the line at 16.8 ppm, characteristic for the intra-octahedral proton.

The peak at 16.8 ppm, which is a single isotropic line without any noticeable spinning sidebands, deserves more attention. As mentioned above, the results of low-temperature solid-state ^2H NMR of the investigated sample could not be analyzed because three signals were observed with three different chemical shift values. Nevertheless, they all contained a narrow line down to 22 K (see Figure 7d). The crucial hint to solve this puzzle is hidden in this temperature dependence. Since motions are not responsible for the disappearance of the quadrupolar interactions, we had to assume that the deuteron is located in a highly symmetric site, where the EFG tensor, which is responsible for the quadrupolar interaction, disappears. Such a site would be the center of the octahedron formed by the six ruthenium atoms. Thus we made the hypothesis that the signal at 16.8 ppm stems from the formation of the side product $[\text{HRu}_6(\text{CO})_{18}]^-$, which can be produced during the synthesis or by the slow deprotonation of $\text{H}_2\text{Ru}_6(\text{CO})_{18}$. In the literature, the measured chemical shift of such a hydrogen environment has been found to be +16.41 ppm.³⁶ To probe this hypothesis, we prepared a sample of solid $[\text{HRu}_6(\text{CO})_{18}]^-$ by deprotonation of $\text{H}_2\text{Ru}_6(\text{CO})_{18}$ upon addition of a stoichiometric amount of NEt_3OH (in methanolic solution). The solid-state ^2H MAS NMR measurements of this sample show a strong signal at +16.8 ppm (see Figure 8). It is noteworthy that this signal is shifted to -15.86 upon re-acidification. These results show that we have indeed found the complex $[\text{HRu}_6(\text{CO})_{18}]^-$, where the deuteron is located inside the metal octahedron.

3.2.2. DFT Calculations. To corroborate these experimental interpretations, DFT calculations were applied. Previous NMR calculations on several $[\text{Ru}_4]$ and $[\text{Ru}_6]$ clusters have proven the ability of DFT to provide accurate chemical shifts for such compounds.⁵⁹ The results for isotropic chemical shifts and quadrupolar interaction parameters are summarized in Table 2. Structure **2a** possesses two conformations of the carbonyl groups (Figure 9), a distorted staggered one (pseudotorision angles of 20–40°) and a nearly eclipsed one (pseudotorision angle of $4 \pm 2^\circ$). The staggered form of the $\text{D}_2\text{Ru}_6(\text{CO})_{18}$ complex, which has a slightly lower absolute energy (~ 2.3 kJ/mol) than the eclipsed form, has a calculated quadrupolar coupling constant of 39 kHz and an asymmetry parameter equal to 0.6. For the

Table 2. Quadrupolar Coupling Constants Q_{cc} , Quadrupolar Splittings Q_{zz} , Asymmetry Parameters η , Absolute Isotropic Magnetic Shielding σ_{iso} , and Isotropic Chemical Shift δ_{iso} Referenced to CD_4 (31.4 ppm) for the Deuterium Nuclei in $\text{D}_2\text{Ru}_6(\text{CO})_{18}$ (**2a,b**), $[\text{DRu}_6(\text{CO})_{18}]^-$ (**2c**), and $[\text{D}_3\text{Ru}_6(\text{CO})_{18}]^+$ (**2d**), Calculated with the 6-31++G(d,p) Basis Set Using the Optimized Structures

complex	Q_{cc} (kHz)	Q_{zz} (kHz)	η	σ_{iso} (ppm)	δ_{iso} (ppm)
2a^a	39.3	29.5	0.60	47.2	-15.8
2a^b	32.6	24.5	0.01	46.7	-15.3
2b^c	17.3	13.0	0.06	27.1	4.3
2b^d	21.5	16.1	0.03	45.9	-14.5
2c	1.13	0.8	0.02	16.0	15.4
2d	30.0	22.5	0.26	43.1	-11.7
	46.1	34.6	0.69	50.8	-19.4
	55.8	41.9	0.92	55.3	-23.9

^a Staggered conformation of **2a**. ^b Eclipsed conformation of **2a**. ^c Deuteron placed inside the Ru_6 octahedron in **2b**. ^d Deuteron placed outside the Ru_6 octahedron in **2b**.

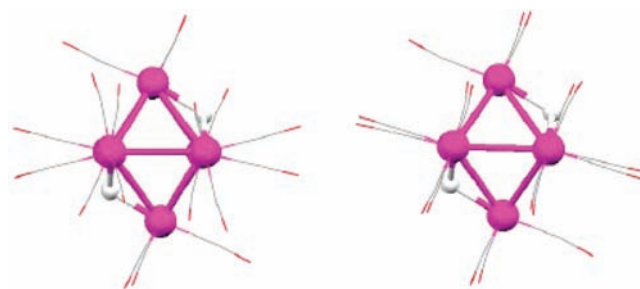


Figure 9. Optimized structures of **2a** calculated with the 6-31++G(d,p) basis set: (left) staggered conformation and (right) eclipsed conformation of the CO groups.

eclipsed conformation the quadrupolar coupling constant and the asymmetry parameter are slightly smaller ($Q_{\text{cc}} \approx 33$ kHz and $\eta \approx 0$).

Comparing these results to the experimental values ($Q_{\text{cc}} \approx 24$ kHz and $\eta \approx 0.2$), it is evident that while the size of the quadrupolar coupling constant is overestimated in both cases,

the asymmetry parameter of the eclipsed conformer is in much better agreement with the experiment than the staggered conformer. This is understandable by the fact that only the eclipsed conformer has a local three-fold symmetry at the hydrogen site. This local three-fold symmetry is distorted in the staggered form, which yields a much higher asymmetry parameter comparable with this one for bridged hydrogen atoms in the $D_4Ru_4(CO)_{12}$ complex (see section 3.1).

Since the eclipsed structure coincides with the X-ray structure determined by Churchill et al.,⁴⁶ we conclude that this structure is the real structure of the complex, despite the slightly higher energy, which is probably an artifact of the DFT calculation at the B3LYP/6-31++G(d,p) level. Detailed theoretical calculations of these structures will be given in a subsequent publication.

For the less symmetric structure **2b**, where one deuteron is placed inside and the other one outside the Ru_6 octahedron, the calculated quadrupolar coupling constant of ~ 21.5 kHz is significantly smaller than for the symmetric structure **2a**. Interestingly, both deuterons exhibit a similar quadrupolar coupling constant which is in the range of 17–22 kHz. The frequency analysis of **2b** however yielded negative frequencies, which indicates a nonminimum geometry of this structure.

The symmetric anion structure of the $[DRu_6(CO)_{18}]^-$ complex **2c** represents a completely different Ru–D binding situation. As the calculations at **2c** show, the quadrupolar coupling constant for the deuteron nearly vanishes, which corroborates well with our experimental interpretation of a deuteron located in the center of a Ru_6 octahedron.

The calculation of the isotropic chemical shifts δ_{iso} (Table 2) at the model structures **2a** and **2b** of the $D_2Ru_6(CO)_{18}$ cluster (respectively **2c** of the $[DRu_6(CO)_{18}]^-$ cluster) shows that deuterons enclosed by ruthenium atoms are highly deshielded, which leads to large positive chemical shifts. In contrast to this fact, the deuterons placed outside the metal octahedron are highly shielded, which yields large negative chemical shift values. Due to the calculated δ_{iso} value for the staggered structure of **2a** (–15.8 ppm), the signal in the MAS spectra with the chemical shift of –15.86 ppm can be attributed to the deuterons in $D_2Ru_6(CO)_{18}$, which proves our signal assignment in the MAS spectra. This calculated δ_{iso} value is also in good agreement with the experimental liquid-state 1H NMR value (15.6 ppm) measured by McCarthy et al.⁶⁰

Due to the possibility of side products of the synthesis, such as $[DRu_6(CO)_{18}]^-$ and $[D_3Ru_6(CO)_{18}]^+$, the chemical shift calculations were performed at the $[DRu_6(CO)_{18}]^-$ cluster **2c** and the $[D_3Ru_6(CO)_{18}]^+$ cluster **2d** (Figure 4). The calculated chemical shift for **2c** (+15.4 ppm), which is similar to both the one measured by Eady et al.³⁶ (+16.41 ppm) and the one measured by us (+16.8 ppm), confirmed that our sample was composed of at least two clusters with different molecular structures. The calculated chemical shift values for the different deuterons in **2d** (–11.7, –19.4, and –23.9 ppm) evidence a strong influence of the carbonyl environment on the chemical shift of the deuteron. If fast motions of these deuterons are expected, their chemical shift values can be averaged. This averaged value (–18.3 ppm) is close to the experimental value of the decomposition product (–20.9 ppm), which supports our assignment of the experimental value of –20.9 ppm to the $[D_3Ru_6(CO)_{18}]^+$ cluster.

3.3. Characteristic Quadrupolar Interactions. Table 3 collects the experimental quadrupolar coupling parameters of the

Table 3. 2H NMR Parameters of Different Compounds Derived from the $D_4Ru_4(CO)_{12}$ (**1**) and the $D_2Ru_6(CO)_{18}$ (**2**) Clusters Found by Line-Shape Analysis of the Spectra (Quadrupolar Coupling Constant Q_{cc} , Asymmetry Parameter η , Isotropic Chemical Shift δ_{iso} , and the Assignments of the Signals) at Different Temperatures

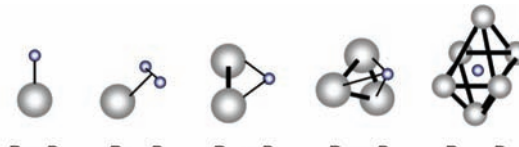
compound	T (°C)	Q_{cc} (kHz)	η	δ_{iso} (ppm)	assignment
$D_4Ru_4(CO)_{12}$	–100	67 ± 1	0.67 ± 0.05	–17.4	Ru_2-D
$D_2Ru_6(CO)_{18}$	rt	24.6 ± 1	0.2 ± 0.1	–15.9	Ru_3-D
$[DRu_6(CO)_{18}]^-$	rt	<2		16.8	Ru_6-D
$[D_3Ru_6(CO)_{18}]^+$	rt	25 ± 4	0.2 ± 0.2	–20.9	Ru_3-D

different types of multinuclear ruthenium complexes. From this table it is evident that there are pronounced differences in Q_{cc} and η for the different binding situations Ru_2-D , Ru_3-D , and Ru_6-D of deuterons in Ru clusters. This shows that solid-state 2H NMR allows a clear distinction between these binding situations in such Ru clusters.

In combination with the data for mononuclear complexes from our previous papers,^{9,23,34} it is now possible to distinguish the different deuterium species $Ru-D_n$ ($n = 1, 2$) and Ru_m-D ($m = 2, 3, 6$) involved in binding to ruthenium by 2H solid-state NMR spectroscopy. Figure 10 summarizes this correlation of typical intrinsic NMR parameters and deuteron binding situation which can be used as a powerful tool for the characterization of hydrogen binding situations in Ru nanoparticles in the future.

4. Summary and Conclusions

Solid-state 2H NMR investigations of the ruthenium clusters $[DRu_6(CO)_{18}]^-$, $D_2Ru_6(CO)_{18}$, $[D_3Ru_6(CO)_{18}]^+$, and $D_4Ru_4(CO)_{12}$ were performed, based on the finding that IR



	Ru–D	Ru–D ₂	Ru ₂ –D	Ru ₃ –D	Ru ₆ –D
n	>3 ^α	>3 ^β	1	1	1
exp. values					
Q_{cc} [kHz]	80–100 ^α	50–80 ^β	≈ 70	≈ 25	≈ 0
η	≈ 0 ^α	≈ 0 ^β	≈ 0.7	≈ 0.2	≈ 0
δ_{iso} [ppm]	-	-	≈ –17	≈ –16	≈ +17
calc. values					
Q_{cc} [kHz]	100–110 ^γ	80–110 ^{**γ}	≈ 80	≈ 35	≈ 1
η	≈ 0 ^γ	≈ 0.5–1 ^γ	≈ 0.7	≈ 0.3	≈ 0
δ_{iso} [ppm]	-	-	≈ –17	≈ –15.5	≈ +15.5

Figure 10. Typical intrinsic NMR parameters of deuterium bound to Ru in model complexes experimentally obtained from low-temperature static powder, respectively MAS NMR experiments, and calculated 2H NMR parameters obtained at the B3LYP/6-31++G(d,p) level of theory. Q_{cc} , quadrupolar coupling constants; η , asymmetry parameters; δ_{iso} , isotropic chemical shifts; n , number of model compounds for which data were obtained. ^αThe large variation in this coupling stems from the range of r_{HH} and r_{RH} distances in different complexes and the presence of chemical exchange and quantum exchange of the deuteron pairs. ^{**}With the exception of the *trans*-[Ru(D₂)Cl(dppe)₂]PF₆ complex,³⁴ where it is possible to determine the static quadrupolar coupling constant, all other experimental quadrupolar coupling constants of the measured samples are reduced by a factor of ca. 2, due to the presence of fast quantum exchange and possibly chemical exchange of the deuteron pairs. ^γ, data refer to additional calculations at the B3LYP/6-31++G(d,p) level of theory employing the model complexes performed in ref 20.

(60) McCarthy, D. A.; Bauer, J. K.; Hong, F. E.; Oh, J. R.; Deng, H. B.; Liu, J. P.; Shore, S. G. *J. Organomet. Chem.* **1998**, *550*, 309.

studies show differences in the spectra which depend on the coordination geometry of the hydrogen (e.g., on-top, the bridging hydrogen, and three-fold hydrogen on the ruthenium surface or octahedral coordination). Differences in the quadrupolar coupling constants Q_{cc} and asymmetry parameters η were obtained for these bonding situations experimentally and theoretically.

Both the quadrupolar coupling constant of $Q_{cc} = 67 \pm 1$ kHz and the asymmetry parameter of $\eta = 0.67$ for deuterium in the tetranuclear ruthenium cluster $D_4Ru_4(CO)_{12}$ differ strongly from the values obtained for mononuclear ruthenium complexes.

From the line-shape analysis of the solid-state 2H MAS NMR spectrum of the hexanuclear $D_2Ru_6(CO)_{18}$ cluster, the quadrupolar interaction for the deuterium bonded to three ruthenium atoms was obtained. The quadrupolar coupling constant and the asymmetry parameter for this binding situation, assigned to the signal with the chemical shift value of -15.86 ppm, were found to be $Q_{cc} = 24.633$ kHz and $\eta = 0.2$. For the octahedral coordination cluster $[DRu_6(CO)_{18}]^-$ a vanishing quadrupolar interaction is found, which is a result of the high symmetry inside the octahedron. The cationic cluster $[D_3Ru_6(CO)_{18}]^+$ exhibits quadrupolar interactions which are close to those of the neutral cluster $D_2Ru_6(CO)_{18}$. DFT calculations at the B3LYP level corroborate these findings.

In combination with the data for the mononuclear complexes, it is now possible to distinguish different hydrogen species $Ru-D_n$ ($n = 1, 2$) and Ru_m-D ($m = 2, 3, 6$) by solid-state 2H NMR spectroscopy, which can act as a powerful tool to characterize the binding situations of hydrogen in Ru nanoparticles or on other metallic surfaces. In a forthcoming theoretical paper, we will shed light on the role of ligands on quadrupolar parameters and define characteristic domains corresponding to each bonding situation summarized in Figure 10.

Acknowledgment. We thank the CNRS, the ANR (SIDERUS project, ANR-08-BLAN-0010-02 and ANR-08-BLAN-0010-03), and DFG under contract Bu-911-12/1 for financial support. T.G. gratefully acknowledges a Ph.D. grant from the state of Thuringia. G.L. thanks Johnson Matthey for complimentary gifts of $RuCl_3 \cdot 3H_2O$, which was used as a starting material. The authors are also grateful to C. Bergounhou and J. F. Pellagatta for assistance in the hydrogenations. T.G. and G.B. thank the Universitätsrechenzentrum Jena, and R.P. and I.d.R. thank the CALcul en MIDI-Pyrénées (CALMIP) and the Centre Informatique National de l'Enseignement Supérieur (CINES) for generous allocations of computer time.

JA104229A